Chapter 5

Proximity induced longitudinal and transverse thermoelectric effect in Gr-$CrBr_3$ van der Waals heterostructure

5.1 Introduction

Proximity effect [1] is one of such emerging interfacial phenomena in layered van der Waals (vdW) crystals enable spellbound possibility in tuning charge transfer aspect for coherent thermoelectric (TE) response. Seebeck effect (SE) represents one of the thermoelectric responses, where conduction of carriers takes place in presence of temperature gradient producing electric signals leading to thermoelectric power generation (TEG) [2-4]. The thermoelectric performance of a material is achieved by determining dimensionless figure of merit, $zT = (\sigma S^2 T)/\kappa$, where σ, S, T and κ are electrical conductivity, Seebeck coefficient, absolute temperature, and thermal conductivity consist of electronic and lattice components [5]. In addition, another thermoelectric behaviour known as anomalous Nernst effect (ANE) emerges from transverse thermoelectric contribution basically observed in ferromagnetic crystals [6]. As compared to conventional Nernst effect, the ANE is observed in presence of temperature gradient with respect to spontaneous magnetization of a ferromagnet (FM) rather than applying any external magnetic field [7,6]. Thus, ANE is considered as a thermoelectric analogue of anomalous Hall Effect (AHE). The TE and ANE are independently studied in hybrid heterostructures such as MoS2/MoSe2 [8], graphene-MoS2 [9], and multilayer graphene nanoplatelets [10]. However, the coexistence of longitudinal and transverse

M Bora and P Deb, *Proximity induced longitudinal and transverse thermoelectric response in graphene-ferromagnetic $CrBr_3$ vdW heterostructure.* J. Phys.: Condens. Matter, 35:055402, 2023.

thermoelectric has been studied in bulk compounds with high external magnetic field and at low temperature [11, 12], limiting its possibility in efficient charge transport. The ANE coefficient for platinum (Pt) on yttrium iron garnet (YIG) has very small value of the magnitude of ~0.06 μV/K [13]. While in real-time picture, Pt/YIG reduce its significance due to short circuit effect; the proximity exists only at the interface and not in the remaining region of Pt/YIG system [13]. The advantage of two-dimensional (2D) materials over bulk counterparts achieves significant improvement in thermoelectric performance due to the discretized electronic structure (quantum confinement) [14]. In addition, proximity coupling with vdW ferromagnet and non-magnetic heterojunctions leads to various interfacial phenomena such as non-trivial phases [15], miniband splitting [16], anomalous nature [17], and band alignment [18]. In this regard, the proximity effect enables to persist distinct order parameters at interface, which further provokes the interaction between the charge carriers and local moment giving rise to TE and ANE in vdW crystals. Therefore, designing robust interface by proximity coupling of vdW crystal will nurture significant progress in recognizing advanced thermoelectric materials.

Graphene gains particular interest as a thermoelectric material due to its extraordinary electrical conductivity and electron mobility [19, 20]. However, pristine graphene exhibits linear dispersion with zero band gap [21] and owns low zT value with large thermal conductivity [22] providing restriction on its applications. In this regard, the theoretical investigation is considered in graphene nanomesh (GNM) [23] and graphene-graphyne nanoribbon heterostructure [24] for enhanced thermoelectric performance by reducing the thermal conductivity. The thermoelectric power factor (PF) can be improved by sandwiching graphene with hexagonal boron nitride (h-BN) due to less potential disturbance with superior electrical conductivity and mobility gradient [25]. The thermoelectric response has high degree of tunability with respect to external perturbations to engineer longitudinal and transverse thermoelectric coefficients [26]. Graphene electronic band structure can be

tuned *via* proximity effect and external perturbative effect, which modify the pristine structure for efficient thermoelectric performance [27]. The external perturbation like electric field gating is quite subtle in vdW heterostructure for modulating the tunnelling probability of Dirac fermions at interface [28]. This contradicts the apprehensions of semimetal to be poor thermoelectric material [29]. As graphene is non-magnetic in nature, it has limitations in realizing anomalous Nernst behaviour. In this regard, magnetic proximity coupling of graphene with 2D ferromagnet will commence efficient charge transfer and interaction with magnetic moments at interface, which further triggers the coexistence of TE and ANE in vdW crystals. This opens a new physical paradigm in generating efficient longitudinal and transverse thermopower simultaneously.

In the current chapter, we explore the presence of TE and ANE with intrinsic origin in vdW heterostructure at room temperature, in view of designing efficient thermopower devices. We consider graphene and ferromagnetic, CrBr3 vdW heterostructure with an interlayer distance of 3.77Å under the framework of ab initio-based density functional theory (DFT) simulations using constant relaxation time approximation (CRTA) utilized from Boltzmann transport equation (BTE). Our theoretical finding illustrates that the Seebeck coefficient is considerably enhanced for the heterostructure. The consistency in conductance spectrum signifies the presence of robust proximity interaction in heterostructure system. The electronic figure of merit suggests that the heterostructure to be an ideal candidate for new generation thermoelectric applications. The oscillatory nature of ANE arises due to presence of proximity interaction in heterostructure system.

5.2 Model and Computational Details

The first-principle based DFT calculation is employed using projector-augmented-wave (PAW) pseudopotential method [30], encoded in Quantum ESPRESSO (QE) package [31]. The Perdew-Burke-Ernzerhoff (PBE) exchange-correlation functional is considered with generalized gradient approximation (GGA) [32]. The cut off energy for plane basis sets is 50 Ry with a vacuum space of 20 Å to ignore interactions among the monolayers. The 9 x 9 x 1 and 27 x 27 x 1 un-shifted K-point sampling are adopted in first Brillouin zone to construct Gr-$CrBr_3$ heterostructure, respectively. The Hellmann-Feynman forces acting on ions is minimized to 0.01 eV/Å. The total energy is calculated with an accuracy of 10^{-8} eV by utilizing Davidson-diagonalization iterative method. For optimum interlayer distance for proximity effect, we introduce van der Waals (vdW) interactions DFT-D2 proposed by Grimme [33]. The optimal interlayer distance is found to be 3.77 Å [16].

To perform the longitudinal and transverse thermoelectric coefficient calculation, we consider linear Boltzmann transport equation (BTE) under the constant relaxation time approach (CRTA) encoded in BoltzTrap2 code [34]. Under this regime, the mean free path of scattered electron is mainly responsible and must be miniaturized than the sample length. In this regard, the conduction of electron and holes will have diffusive nature and Boltzmann approach is absolute to characterize the transport phenomena. Considering CRTA approach, thermoelectric behaviour can be elaborated from transport coefficient using TE kernel integration, $L_n = \int_{-\infty}^{\infty} T(E)(E-\mu)^n \left(\frac{-\partial f}{\partial E}\right) dE$, here, *T(E)* describes the transport distribution function (TDF), μ represents chemical potential, *f(E)* is Fermi-Dirac distribution. The TDF can be written as, $T(E) = v^2(E)\tau(E)g(E)$, here, v describes the velocity, $\tau(E)$ depicts relaxation time and $g(E)$ is density of states (DOS).

Under CRTA scheme, DOS is indirectly proportional to relaxation time and can be expressed as, $g(E) = \frac{C}{\tau(E)}$, where C refers to the scattering coefficient. In this case, the velocity will be expressed in terms of group velocity $v^2(E) = v_g^2/2$. The transport coefficient for each electronic structure will be considered with consummate boundary conditions. Under Boltzmann transport theory within CRTA, the transport coefficients of longitudinal thermoelectric property can be expressed as, $S = \frac{1}{qT}\frac{L_1}{L_0}$, $\sigma = q^2 L_0$, $\kappa_e = \frac{1}{T}(L_2 - \frac{(L_1)^2}{L_0})$. Here, e is the electronic charge and T is the absolute temperature. Moreover, the transverse part of the thermoelectric coefficient can be written as, $\alpha_{xy}(T, \mu) = \frac{1}{e}\int dE\,(-\frac{df}{dE})\sigma_{xy}(0, E)\frac{E-\mu}{T}$. The integration was calculated by introducing the energy dispersion (E) with respect to electronic wave vector $\boldsymbol{k}$ obtained from the first-principle DFT calculation.

5.3 Result and Discussions

5.3.1 Thermodynamic stability

For quantitative measurement, the thermodynamic stability of stacked Gr-$CrBr_3$ vdW heterostructure is achieved as shown in figure 5.1. We determine the binding energy (E_b) of heterostructure system as per the concerned equation, $E_b = \frac{[E_{Grp-CrBr_3} - (E_{Grp} + E_{CrB_3})]}{N}$, where, $E_{Grp\text{-}CrBr3}$, E_{Grp} and E_{CrBr3} and N represent the total energies of Gr-$CrBr_3$ heterostructure, pristine graphene, $CrBr_3$ monolayers and number of atoms in corresponding unit cell (N=22), respectively. The calculated binding energy is found to be -26 meV. The negative binding energy signifies the heterostructure formation to be thermodynamically stable. The optimized interlayer spacing between graphene and $CrBr_3$ is 3.77 Å, which is evident from the binding energy versus interplanar spacing plot as shown in figure 5.1 (c).

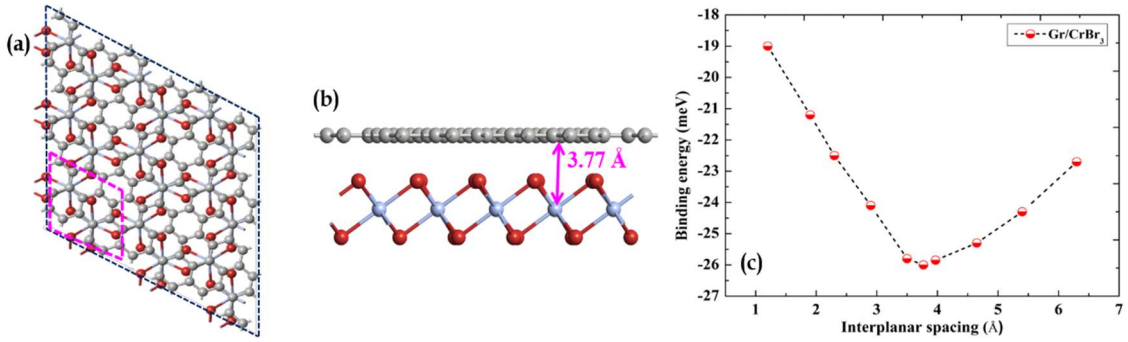

Figure 5.1: Atomic structure of Gr-$CrBr_3$ vdW heterostructure. The grey, blue and red balls represent carbon (C), chromium (Cr) and bromine (Br), respectively. The pink dashed box indicates the unit cell of Gr-CrBr3 heterostructure. (a) Top-view and (b) side view. The interlayer distance for possible proximity integration is 3.77 Å. (c) Calculated binding energy with respect to interplanar spacing of Gr-$CrBr_3$ vdW heterostructure

5.3.2 Electronic property

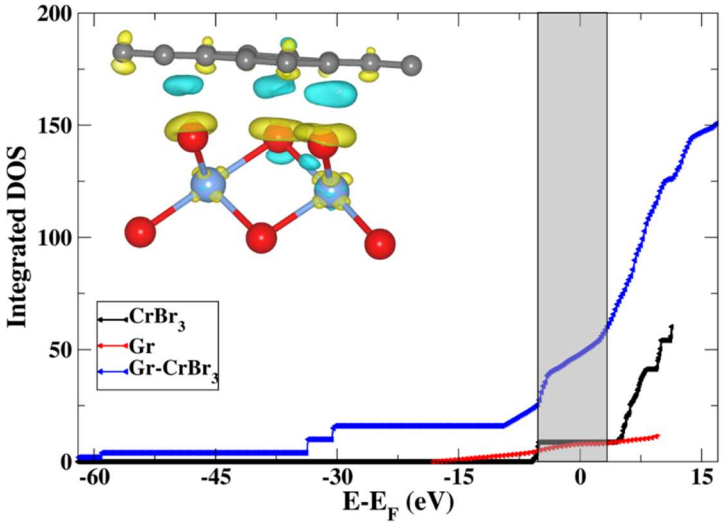

Figure 5.2: Calculated integrated DOS for Gr-$CrBr_3$ vdW heterostructure system. The black, red and blue solid lines depict total integrated DOS for $CrBr_3$ monolayer, graphene monolayer and Gr-$CrBr_3$ bilayer, respectively. The inset displays the charge density difference (CDD) for bilayer system with isosurface value ± 0.0025 e/Å^3, where yellow and cyan colour represents positive and negative isosurface value, respectively.

The calculated integrated DOS is plotted for monolayer graphene, monolayer $CrBr_3$ and Gr-$CrBr_3$ vdW heterostructure as shown in figure 5.2. The red, black and blue solid lines represent total integrated DOS for graphene, $CrBr_3$ and the heterostructure system, respectively. Due to proximity coupling, the heterostructure exhibit characteristic of linear Dirac band dispersion from graphene as well as finite band gap of 0.8 eV from $CrBr_3$ monolayer, which is pertinent with prior study [16, 35]. The graphene Dirac point is observed at conduction band minimum (CBM) of $CrBr_3$, which represent the semimetallic-semiconductor characteristic of electronic bands. The integrated DOS pattern for heterostructure system near the Fermi level basically comprises mixed character of graphene and $CrBr_3$ leading to efficient conduction of electrons and holes, contributing directly to realize thermoelectric (TE) behaviour of the heterostructure system. Moreover, in integrated DOS pattern, monolayer graphene and $CrBr_3$ observes no certain elevation at the Fermi region. Therefore, transport properties for holes contribution are dominated by graphene while electrons contributions are characterized by both graphene and ferromagnetic $CrBr_3$. The inset shows the differential charge density distribution (CDD) for Gr-$CrBr_3$ heterostructure system, where yellow and cyan colour depicts positive and negative charge i.e., the conduction of holes and electrons at the interface and accumulation of charges at surface of bilayer system. The charge transfer is observed in partial regions due to electrostatic screening effect arise in bilayer system. This robustness signifies the presence of MPE and deduces TE properties in heterostructure system.

5.3.3 Conductance

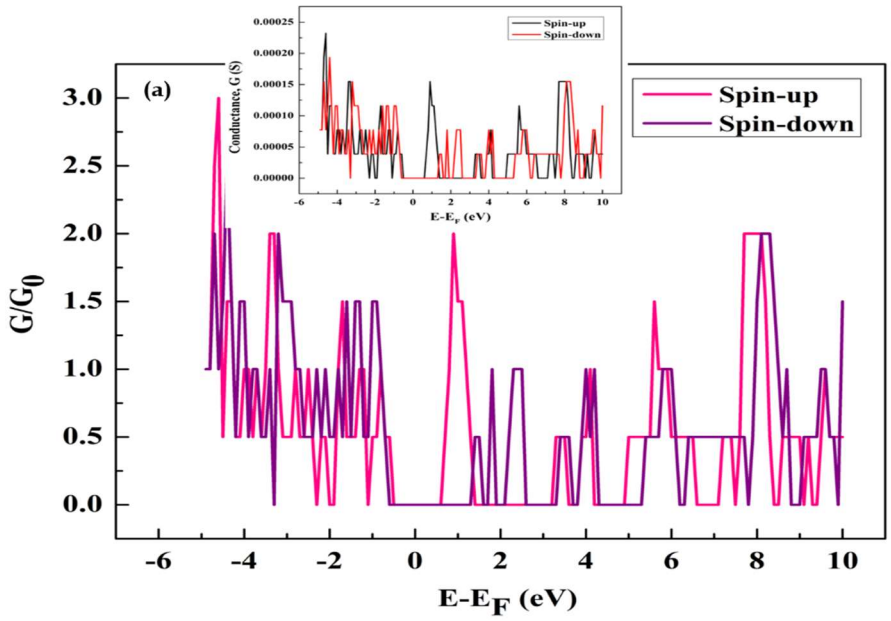

Figure 5.3: Spin-polarized normalized conductance for heterostructure as a function of Fermi energy. The pink and violet lines depict spin-up and down states, respectively. The inset represents the spin-polarized conductance with respect to Fermi energy.

Figure 5.3 displays normalized spin-polarized conductance (G/G_0) as a function of Fermi energy for the heterostructure system. To realize the presence of MPE, spin-polarized transport phenomena has been calculated at interface of heterostructure system via non-equilibrium Greens' function (NEGF) process. The spin-up conductance value for energy interval 0-2 eV is found to be 2, while for spin-down states it is 0.5. Therefore, asymmetric nature is clearly evident from normalized conductance spectrum for respective spin configurations. The spectrum displays the step-like nature from valence to conduction band in Gr-$CrBr_3$ heterostructure. This step-like conductance spectrum remains consistent for both spin-up and spin-down configurations, respectively. The consistent nature of spectrum influences interfacial polarization of electrons due to active proximity coupling. The inset also confirms the asymmetric behaviour with conductance value of 155 μS and 39 μS for spin-up and down states, respectively at energy interval of 0-2 eV.

5.3.4 Thermoelectric behaviour

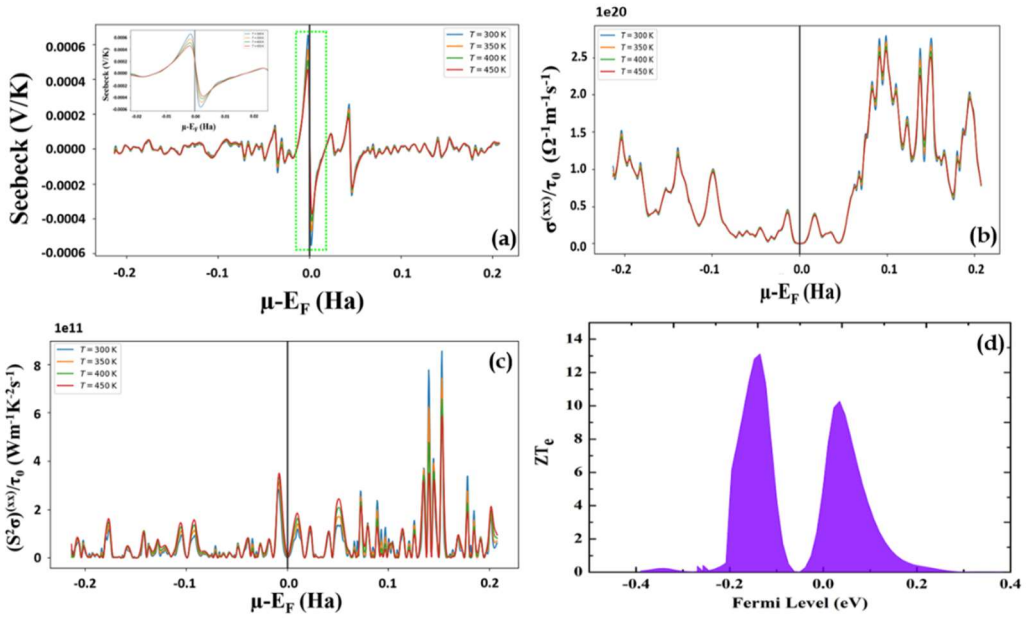

Figure 5.4: (a) The calculated Seebeck coefficient with respect to chemical potential at temperature 300 K to 450 K for Gr-$CrBr_3$ van der Waals heterostructure. (b) Calculated electrical conductivity and (c) Calculated power factor for Gr-$CrBr_3$ bilayer system as a function of chemical potential. (d) The electronic figure of merit with respect to the Fermi level at 300 K for the heterostructure system at zero bias.

Figure 5.4 (a) presents the calculated Seebeck coefficient (S_{xx}) as a function of chemical potential, temperature varying from 300-450 K for Gr-$CrBr_3$ vdW heterostructure by implementing Boltzmann transport equation (BTE) using BoltzTrap2 code under constant relaxation time approach (CRTA). The coefficient alters substantially with respect to chemical potential, estimating an optimum carrier concentration is favorable to accomplish thermoelectric performance of the heterostructure system. Near the Fermi level (μ=0), the Seebeck coefficient prevail two obvious peaks for both p- and n-type concentrations. The estimated Seebeck coefficient $|S_{xx}|$ is found to be 653μV/K at 300 K and the value of coefficient decreases up to 400μV/K at 450 K. The Seebeck coefficient value decreases with increase in temperature due to increase in electron energy as compared to its change created by means of temperature

gradient. Also, this effect is because of bipolar conduction effect or the stimulation of carriers of both positive and negative charge implying the inverse Hall coefficient [36]. As Seebeck coefficient is related to band structure, the band structure shows semimetal-ferromagnetic semiconductor characteristic due to MPE at high-symmetry point leading to asymmetric nature with minimum overlap of electrons and holes in the electronic properties of Gr-$CrBr_3$ bilayer system. This asymmetric nature of bands in heterostructure system leads to high S value at room temperature by interacting charge carriers with magnetic moments of ferromagnetic $CrBr_3$, which provides heat-driven electron transport and consequently enhances thermopower.

Based on the calculated electronic band structure, the transport coefficients from the electronic contribution for Gr-$CrBr_3$ heterostructure system is evaluated within the semi-classical BTE and rigid band model. To obtain accurate results, we consider a highly dense *k* mesh in irreducible Brillouin zone (IBZ) for the heterostructure system. The semi-classical BTE rely on the ratio σ/τ corresponding to nine diagonal components of conductivity tensor. Using the ratio σ/τ component of conductivity tensor, the relaxation time can be considered as 10^{-14} within the permissible range [37]. In this regard, scaling of S_{xx} and σ can be utilized *via* relaxation time constant τ. The electrical conductivity is obtained when the relaxation time parameter is considered into all components of σ/τ. Figure 5.4 (b) displays the electrical conductivity with respect to chemical potential μ at varied temperatures. Unlike the Seebeck coefficient the electrical conductivity is less dependent on temperature. The Seebeck value and electrical conductivity is inversely proportional to each other. In this regard, we observe near the Fermi level the conductivity is less but the magnitude of Seebeck value is higher. It is also seen that the conductivity in n-type chemical potential region is of the order of 2.8×10^6 S/m, which is higher as compared to Seebeck value in n-type chemical potential region. The electrons are dominant carrier in Gr-$CrBr_3$ heterostructure system, which plays active

role in conduction. Therefore, the trade-off is clearly evident between Seebeck and electrical conductivity for Gr-$CrBr_3$ heterostructure system. The measured electronic thermal conductivity also follows the same trend as electrical conductivity relying on Wiedemann-Franz law as shown in appendix figure A2. Subsequently, electronic power factor (PF) is plotted relative to chemical potential in Figure 5.4 (c) at different temperatures. The power factor is the product of square of Seebeck value and electrical conductivity. The maximum value of PF is 8.5×10^{11} $Wm^{-1}K^{-1}s^{-1}$ for positive chemical potential (n-type carrier concentration) at room temperature.

Figure 5.4 (d) displays the dimensionless figure of merit for electronic contribution as a function of Fermi energy at room temperature. This dimensionless quantity is calculated considering power factor, temperature and electronic thermal conductivity to examine the energy conversion efficiency. In this calculation, we have neglected the lattice thermal conductivity from phonon contribution in 2D heterostructure system because phonons actively participate as heat carriers in bulk solids. In such heterostructure system, the phonon scattering increases and its contribution to lattice thermal conductivity dramatically decreases due to reduced dimensionality. This significantly changes the phonon dispersion as well as density of states for low-dimensional systems. Therefore, the reasonable approximation by omitting lattice thermal conductivity will lead to higher figure of merit value considering the contribution of electronic thermal conductivity [37]. It is evident that calculated figure of merit from electronic contribution attains two peaks at room temperature, with uttermost value of 13.10 at -0.13 eV and 10.21 at 0.034 eV, suggests remarkable ZT_e value through doping in heterostructure system.

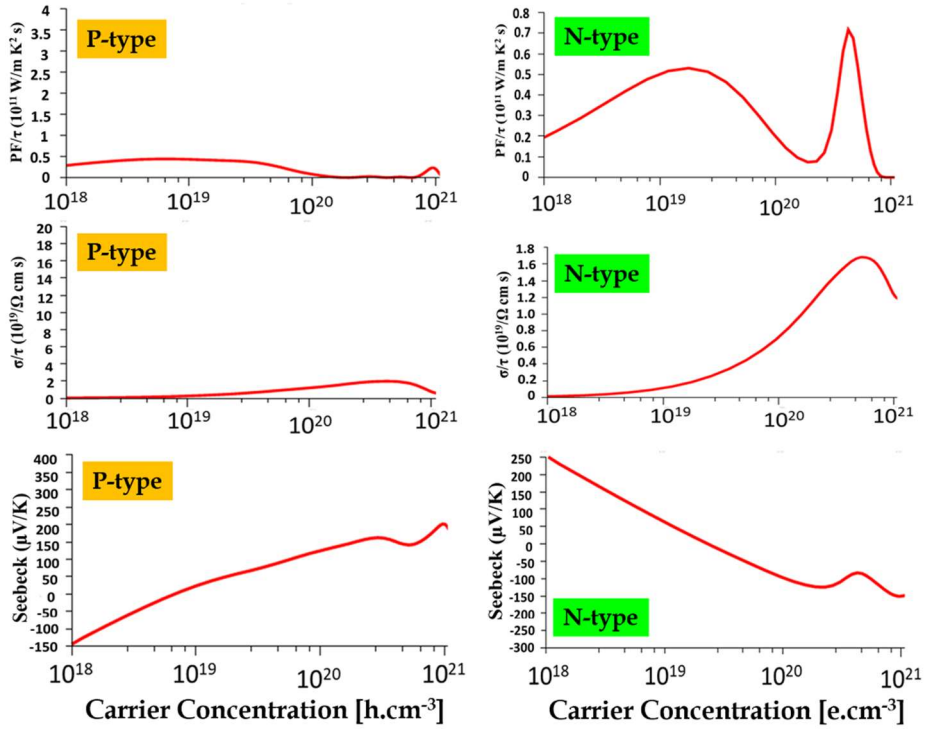

Figure 5.5: Left panel describes (a) the power factor, (b) electrical conductivity and (c) Seebeck coefficient with respect to hole-doping concentration at temperature in no bias at 300 K for Gr-$CrBr_3$ van der Waals heterostructure. Right panel displays (d) the power factor, (e) electrical conductivity and (f) Seebeck coefficient as a function of electron-doping concentration at zero bias at room temperature.

Figure 5.5 displays the calculated PF ($S^2\sigma/\tau$), electrical conductivity (σ/τ) and Seebeck coefficient (S_{xx}), where τ is the relaxation time for Gr-$CrBr_3$ heterostructure system with respect to doping concentration at 300 K. From figure 5.4 (left and right panel) it is clearly evident that hole concentration (p-type) is contributing minorly to the conductivity whereas electron concentration (n-type) is contributing significantly of the order of n_e = ~10^{20} cm^{-3} at 300 K and follows the trend of ideal thermoelectric (TE) material. The contribution of electron concentration indicates the Gr-$CrBr_3$ heterostructure to be n-type TE material. The majority of electron contribution is also confirmed from Figure 5.4 and correlates well with it. Figure 5.5 (c) and (f) The Seebeck coefficient with respect to electron concentration is found to be -150μV/K at a concentration of n_e = ~10^{20} cm^{-3} and 100μV/K for n_h = ~10^{20} cm^{-3} at 300 K. Therefore, Seebeck

coefficient value in the heterostructure system is higher in electron concentration than hole-carrier concentration, which confirms the system exhibits n-type TE properties.

The dependence of electrical conductivity is plotted with respect to hole-carrier concentration and electron carrier concentration for Gr-$CrBr_3$ vdW bilayer system in figures 5.5 (b) and (e). The electrical conductivity in electron carrier concentration (shown in figure 5.5 (e)) is infinitesimally higher than that of the hole carrier concentration (shown in figure 5.5 (b)) in heterostructure system. The enhancement in electrical conductivity can be explained on the basis of two reasons. Firstly, the elevation at the Fermi level leads to non-zero value in integrated DOS pattern can possibly estimate the increase in carrier concentration and would enhance the electrical conductivity for electron carrier. Secondly, conduction of charge from one layer to neighbouring layer. To illustrate the conduction of charge among the layers, we plotted integrated DOS as a function of Fermi energy region for monolayers as well as the heterostructure system. The integrated DOS specifically confers the probability of electron density present in conduction band region and holes in valence band of unit cell. The calculated ratio from integrated DOS for monolayer $CrBr_3$ to monolayer graphene is about 1.55, while the ratio of integrated DOS for bilayer system to that of monolayer $CrBr_3$ and graphene is 1.66. The ratio for the bilayer system is higher than that of the monolayer $CrBr_3$ and graphene. This clearly signifies the presence of charge transfer from partial regions of graphene to $CrBr_3$ layer, which can also be confirmed from the inset of figure 5.2. As a consequence of charge transfer there will be elevation in electron and hole carrier concentration, which improves the electrical conductivity for electron carrier in Gr-$CrBr_3$ heterostructure.

The calculated PF ($S^2\sigma/\tau$) is plotted with respect to the carrier concentration as shown in figure 5.5 (a) and (d), under the energy-liberated relaxation time τ scheme. The carrier concentration dependent PF is obtained for Gr-$CrBr_3$ heterostructure system shows peak at electron carrier concentration n_e~$0.5x10^{20}$ cm^{-3} and hole carrier concentration n_h~$0.25x10^{19}$ cm^{-3}. The power factor value in case of electron concentration is substantially higher than that of hole-carrier concentration. In this regard, electronic structure is an important factor for resonating electron-hole conduction to describe TE behaviour in heterostructure system.

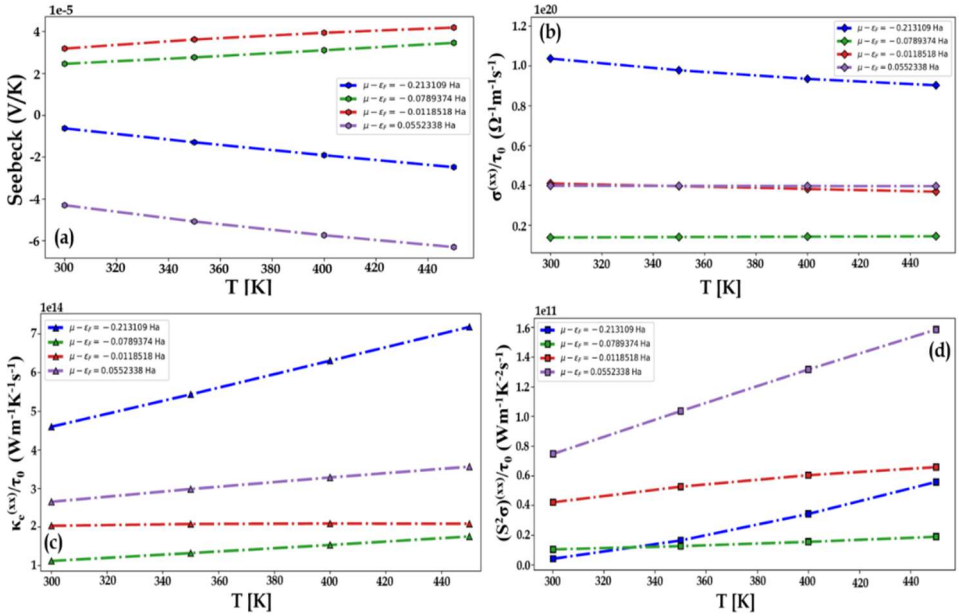

Figure 5.6: Temperature dependence of (a) Seebeck coefficient, (b) electrical conductivity, (c) electronic thermal conductivity (κ_e), and (d) power factor of Gr-$CrBr_3$ vdW heterostructure at different chemical potential.

Temperature dependent Seebeck coefficient is plotted as shown in figure 5.6 (a) at different chemical potential, which displays an intriguing n-p type transition with increase in temperature. The value of Seebeck coefficient usually explicate by Mott equation [38], relating to the derivative of logarithmic function of electrical conductivity can be expressed as, $S = \frac{\pi^2}{3}\left(\frac{k_B^2 T}{g}\right)\left[\frac{\partial \ln \sigma(E)}{\partial E}\right]_{E=E_F} = \frac{\pi^2}{3}\left(\frac{k_B^2 T}{g}\right)\left[\frac{1}{n}\frac{\partial \ln (E)}{\partial E} + \frac{1}{\mu}\frac{\partial \mu(E)}{\partial E}\right]_{E=E_F}$ where, $\mu(E)=g\tau(E)/m^*$ is the energy dependent

chemical potential for carrier mobility, g is charge of carrier, T denotes temperature, k_B is the Boltzmann constant, m^* describes effective mass and E_F is Fermi energy. The Mott relation says that Seebeck value decreases with the elevation in doping concentration, which is also evident from figure 5.5. The n-p type transition in Seebeck coefficient is non-uniform suggesting the creation of potential at the interface between monolayers graphene and $CrBr_3$ because of proximity integration, where the carriers having low kinetic energy are removed by energy barrier at interface due to the shifting of Fermi level and carriers exhibiting high kinetic energy are considered for transport phenomena. This behaviour can be explained by charge carrier filtering effect [39, 40], which occurs basically at the interface.

Figure 5.6 (b) and (c) describes the electrical conductivity and electronic thermal conductivity as a function of temperature at different chemical potentials considering constant relaxation time. The trade-off between Seebeck, electrical and electronic thermal conductivity is well established and corroborates well with figures 5.4 and 5.5. It is evident from figure 5.6 (c), the κ_e value increases with increase in temperature for μ=-0.213109 Ha. Due to the increase in temperature the charge carrier will suffer higher thermal energy and propagate free electrons creating holes from valence to conduction band region. The electrical conductivity for heterostructure system (shown in figure 5.6 (b)) shows a consistent nature with the increase in temperature. The value of σ_e for μ=-0.213109 Ha is about 1.0×10^{20} $\Omega^{-1}m^{-1}s^{-1}$ at 300 K and slightly decreases with the increase in temperature. Due to the slight overlap in semimetal-ferromagnet heterojunction, the vibration in metal ions increases resulting in increase of resistance in the heterojunction. However, in other chemical potentials the electrical conductivity is consistent throughout the temperature range because of seamless proximity integration giving rise to asymmetric bands and density of states. As a consequence, this consistent nature of electrical conductivity is worth to mention for smooth and continuous diffusion of charge carriers at the heterojunction making it suitable for efficient charge transport. The temperature

dependent power factor is plotted (shown in figure 5.6 (d)) at various chemical potentials. The power factor value at μ=0.0552338 Ha has higher value as compared to other chemical potential due to high Seebeck and electrical conductivity value of heterostructure system.

5.3.5 Anomalous Nernst Effect (ANE)

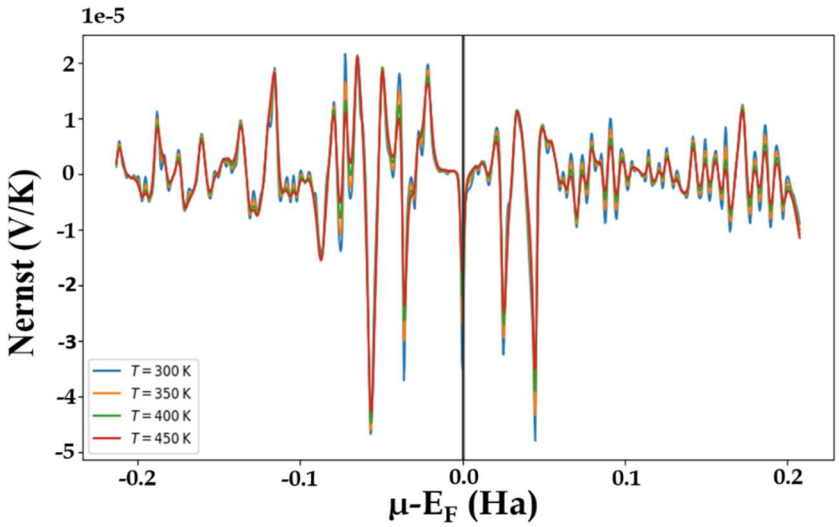

Figure 5.7: Dependence of anomalous transverse thermopower (anomalous Nernst thermopower, S_{xy}) as a function of chemical potential observed in Gr-$CrBr_3$ vdW heterostructure at different temperatures from 300-450 K.

The occurrence of anomalous Nernst effect (ANE) is a part of transverse TE effect in presence of ferromagnet without applying any external magnetic field [6]. In this case, monolayer graphene and monolayer $CrBr_3$ are coupled magnetically *via* proximity effect; hence, no external magnetic field is applied. Figure 5.7 shows the dependence of anomalous transverse thermopower with respect to chemical potential at different temperature from 300-450 K. At the Fermi region, μ=0, $|S_{xy}|$=40 μV/K at 300 K. As the temperature increases above room temperature, the transverse thermopower decreases at Fermi region is found to be ~20μV/K. It is observed that calculated value of transverse thermopower is obtained on the basis of intrinsic origin due to magnetic proximity coupling between graphene and ferromagnetic $CrBr_3$. As seen from

the figure, it is clearly evident that oscillatory behaviour is detectable throughout from negative to positive chemical potential. Moreover, oscillatory behaviour of Nernst effect was previously observed by doping [41] or externally applying magnetic field [42] in quantum systems. Such oscillatory behaviour gives rise to quantum oscillations in Gr-$CrBr_3$, which is observed intrinsically due to seamless proximity integration without any external magnetic field leading to realize anomalous Nernst behaviour.

5.3.6 Variation of electric field in thermoelectric behaviour

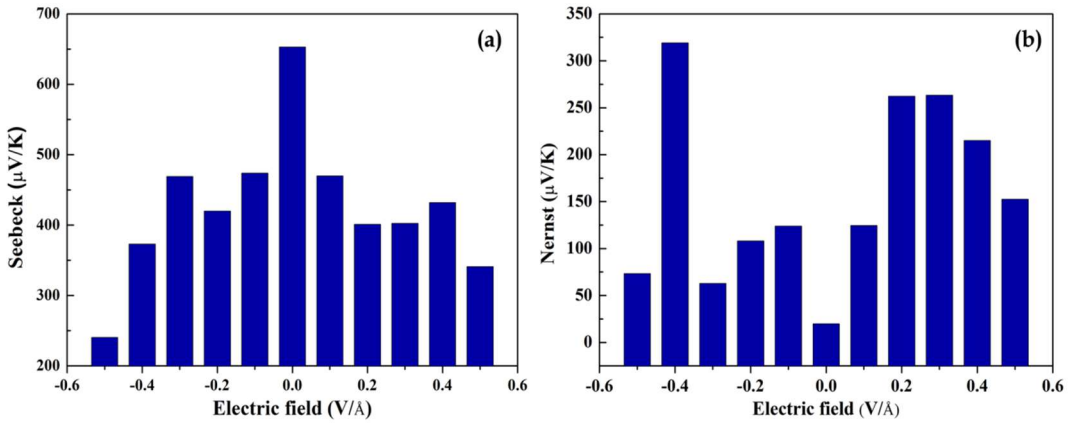

Figure 5.8: Dependence of (a) Seebeck effect (S_{xx}) and (b) anomalous transverse thermopower (anomalous Nernst thermopower, S_{xy}) as a function of applied electric field (-0.5 V/Å to 0.5 V/Å) in Gr-$CrBr_3$ vdW heterostructure at room temperature.

The compulsion of Seebeck effect (S_{xx}) is addressed with respect to applied electric field at room temperature as shown in figure 5.8 (a) for Gr-$CrBr_3$ vdW heterostructure. It is observed that S_{xx} is quite sensitive towards applied electric field due to the fluctuation in split-off energy obtained previously [16]. Thus, prominent non-linearity is evident with implications of applied electric field from 0 to ±0.5 V/Å leading to rapid diffusion of charge carriers screened from $CrBr_3$ to graphene layer and electron-hole recombination. As seen from figure 5.8 (a), it is clearly seen that the Seebeck coefficient (S_{xx}) is responsive with the modulation of electric field because of interlayer polarization effect. It is seen that the S_{xx} value decreases with external biasing as compared to zero biasing

(shown in figure 5.5) due to in-built electric field produce between graphene and $CrBr_3$ monolayers creating entropy difference by recombining charge carriers at the interface, which can possibly tune charge transport *via* proximity interaction. The trade-off between Seebeck and electrical conductivity, power factor is also consistent with the application of electric field revealing the heterostructure system to be an ideal thermoelectric material.

Unlike Seebeck effect, in anomalous Nernst effect the intrinsic magnetism truncates electrons and holes to divert in opposite directions. Thus, both the carriers promote transverse TE properties. It is clearly seen from figure 5.8 (b), distinct non-linearity is observed like Seebeck effect (shown in figure 5.8 (a)) with applied electric field. However, the trend of non-linearity for ANE is different from Seebeck effect based on intrinsic origin (MPE) i.e. at zero bias S_{xx} (S_{xy}) is showing a greater (lower) value of 653μV/K (40μV/K). This trade-off can be possibly due to the shift in Fermi energy with applied biasing observed previously in electronic bands [43], which can be explained on the thrust of rigid-band model [43]. In addition, it is seen that S_{xy} is enhanced with applied biasing compared to zero bias due to its tunability in Fermi level, which is an important factor to boost ANE in Gr-$CrBr_3$ heterostructure system. As S_{xy} increases with applied bias, the interaction between charge carriers and local magnetic moment between graphene and ferromagnetic $CrBr_3$ monolayers, which can be quantified on the basis of skew-scattering or side-jump mechanism [43]. Therefore, modulation of Fermi level in transverse (ANE, S_{xy}) and longitudinal (Seebeck, S_{xx}) thermopower with respect to applied electric field provides high degree of tunability in Gr-$CrBr_3$ heterostructure system.

5.3.7 Device prototype

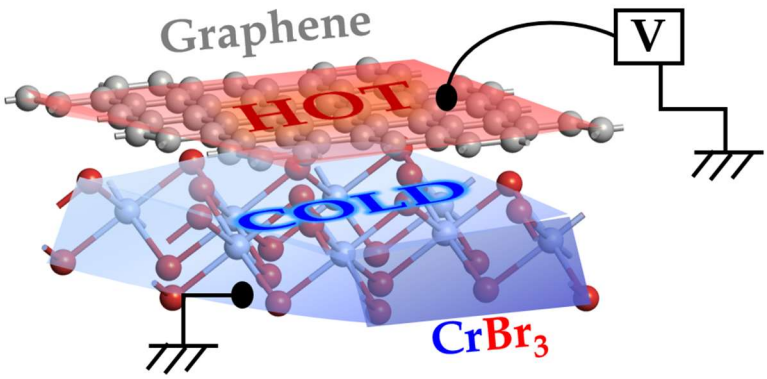

Figure 5.9: Thermoelectric device prototype of Gr-$CrBr_3$ vdW heterostructure, where graphene monolayer act as a hot and $CrBr_3$ monolayer as a cold junction, respectively.

Figure 5.9 illustrates the proposed vdW heterostructure-based thermoelectric prototypic device model composed of two monolayers graphene at the top and bottom layer consist of ferromagnetic $CrBr_3$ proximity coupled with an interlayer distance of 3.77 Å. The proposed device can either generate power or refrigerate relying on the flow of charge carriers. If electron mobility occurs from hot to cold throughout the heterojunction, then the system will generate power. When the two monolayers are proximity coupled with each other, the charge carriers flow from partial regions of heterostructure creating a temperature gradient basically from graphene (hot region) to $CrBr_3$ (cold region) electrostatically screened from chromium atom leading to interlayer polarization for tranquil motion of electrons at the interface. In this regard, entropy charge occurs due to different thermal energies at both ends integrated with charge carrier mobility at Fermi energy in heterostructure system. When the bias voltage is applied, conduction of electron and holes increases due to the polarization effect and shifting of Fermi energy is prominent at the electronic structure [16]. Therefore, thermoelectric effect can be easily driven by interlayer polarization and entropy difference under a thermal energy regime due to

active proximity effect making it feasible for developing energy harvesting device.

5.4 Concluding remarks

In conclusions, we investigated thermoelectric behaviour and observed anomalous Nernst effect (ANE) in Gr-$CrBr_3$ vdW heterostructure relying on the variation of carrier concentration and temperature based on DFT calculations and utilizing semi-classical Boltzmann transport equation (BTE). The Seebeck coefficient is found to be 653 μV/K near Fermi level at room temperature, which is much higher than that of pristine monolayers. The trade-off between Seebeck, electrical and electronic thermal conductivity is clearly evident in the heterostructure system. The charge transfer is observed from the partial regions at the interface from graphene to $CrBr_3$ due to proximity interaction. The elevation at the Fermi level is observed in integrated DOS leading to smooth conduction of electron and holes making it feasible for charge transport phenomena. The power factor, Seebeck and electrical conductivity are found to be majorly dominated by electron concentration and minority holes concentration. In this regard, Gr-$CrBr_3$ heterostructure system exhibits n-type thermoelectric behaviour. The spin-polarized conductance signifies the asymmetric nature and persists step-like spectrum for both spin-configurations due to active proximity integration. Moreover, the conductance value of 155 μS and 39 μS is obtained for spin-up and down states, respectively. The dimensionless electronic figure of merit (ZT_e) is obtained as 13.10 at -0.13 eV and 10.21 at 0.034 eV, suggesting the heterostructure system to be an ideal thermoelectric material. In addition, anomalous Nernst effect (ANE) is observed with an oscillatory nature in heterostructure system. The oscillatory behaviour is determined on the basis of intrinsic origin, where the charge carriers interact with the magnetic moment of $CrBr_3$ layer due to proximity effect. Moreover, the Seebeck effect and ANE is sensitive to the application of external electric field. Our findings determine Gr-$CrBr_3$ as an ideal system for thermoelectric material

and realize anomalous behaviour for developing energy efficient nanoscale devices.

References

[1] Bora, M. and Deb, P. Magnetic proximity effect in two-dimensional van der Waals heterostructure. *Journal of Physics: Materials*, 4:034014, 2021.

[2] Poudel, B., Hao, O., Ma, Y., Lan, Y., Minnich, A., Yu, B., Yan, X., Wang, D., Muto, A., Vashaee, D., Chen, X., Liu, J., Dresselhaus, M. S., Chen, G. and Ren, Z. High-Thermoelectric performance of nanostructured Bismuth Antimony Telluride Bulk alloys. *Science*, 320:634, 2008.

[3] Chu, S., Cui, Y. and Liu, N. The path towards sustainable energy. *Nature Materials*, 16:16-22, 2017.

[4] Behera, S. K. and Deb, P. PAW mediated *ab initio* simulations on linear response phonon dynamics of anisotropic black phosphorous monolayer for thermoelectric applications. *Physical Chemistry Chemical Physics*, 20:26688, 2018.

[5] Majumdar, A. Thermoelectricity in semiconductor nanostructures. *Science*, 303:777, 2004.

[6] Ramos, R., Aguirre, M. H., Anadon, A., Blasco, J., Lucas, I., Uchida, K., Algarabel, P. A., Morellon, L., Saitoh, E and Ibarra, M. R. Anomalous Nernst effect of Fe_3O_4 single crystal. *Physical Review B*, 90:054422, 2014.

[7] Boona, S. R., Myers, R. C. and Heremans, J. P. Spin caloritronics. *Energy & Environmental Science*, 7:885, 2014.

[8] Jia, P. -Z. et al. Excellent thermoelectric performance induced by interface effect in MoS2/MoSe2 van der Waals heterostructure. *Journal of Physics: Condensed Matter*, 32:055302, 2020.

[9] Kim, S., Lee, C., Lim, Y. S. and Shim, J-H. Investigation for thermoelectric properties of the MoS2 monolayer-graphene heterostructure: Density functional

theory calculations and electrical transport measurements. *ACS Omega*, 6:278, 2021.

[10] Lin, Y., Wood, M., Imasato, K., Kuo, J. J., Lam, D., Mortazavi, A. N., Slade, T. J., Hodge, S. A., Xi, K., Kanatzidis, M. G., Clarke, D. R., Hersam, M. C. and Snyder, G. J. Expression of interfacial Seebeck coefficient through grain boundary engineering with multi-layer graphene nanoplatelets. *Energy & Environmental Science*, 13:4114, 2020.

[11] Hirokane, Y., Tomioke, Y., Imai, Y., Maeda, A. and Onose, Y. Longitudinal and transverse thermoelectric transport in MnSi. *Physical Review B*, 93:014436, 2016.

[12] Feng, T. et al. Large Transverse and Longitudinal Magneto-Thermoelectric Effect in Polycrystalline Nodal-Line Semimetal Mg_3Bi_2. *Advanced Materials*, 34:2200931, 2022.

[13] Guo, G. Y., Niu, Q. and Nagaosa, N. Anomalous Nernst and Hall effects in magnetized platinum and palladium. *Physical Review B*, 89:214406, 2014.

[14] Wu, J., Chen, Y., Wu, J. and Hippalgaonkar, K. Perspectives on Thermoelectricity in Layered and 2D materials. *Advanced Electronic Materials*, 4:1800248, 2018.

[15] Mohanty, S. and Deb, P. Nontrivial band topology coupled thermoelectrics in $VSe_2/MoSe_2$ van der Waals magnetic Weyl semimetal. *Journal of Physics: Condensed Matter,* 34:335801, 2022.

[16] Behera, S. K., Bora, M., Chowdhury, S. S. P. and Deb, P. Proximity effects in graphene and ferromagnetic $CrBr_3$ van der Waals heterostructures. *Physical Chemistry Chemical Physics,* 21:25788, 2019

[17] Bora, M., Behera, S. K., Samal, P. and Deb, P. Magnetic proximity induced valley-contrasting quantum anomalous Hall effect in a graphene-CrBr3 van der Waals heterostructure. *Physical Review B,* 105:235422, 2022.

[18] Talukdar, M., Behera, S. K., Jana, S., Samal, P. and Deb, P. Band alignment at heterointerface with rapid charge transfer supporting excellent photocatalytic degradation of methylene blue under sunlight. *Advanced Material Interfaces*, 9:2101943, 2022.

[19] Xu, Y., Li, Z. and Duan, W. Thermal and thermoelectric properties of Graphene. *Small,* 10:2182, 2014.

[20] Jin, Q. et al. Flexible layer-structure Bi_2Te_3 thermoelectric on a carbon nanotube scaffold. *Nature Materials*, 18:62−68, 2019.

[21] Schwierz, F. Graphene transistors. *Nature Nanotechnology,* 5:487, 2010.

[22] Balandin, A. A., Ghosh, S., Bao, W., Calizo, I., Teweldebrhan, D., Miao, F. and Lau, C. N. Superior thermal conductivity of single-layer Graphene. *Nano Letters,* 8(3):902, 2008.

[23] Gunst, T., Markussen, T., Jauho, A. -P. and Brandbyge, M. Thermoelectric properties of finite graphene antidote lattices. *Physical Review B,* 84:155449, 2011.

[24] Zhou, J. and Li, D. Improving the thermoelectric properties of graphene through zigzag graphene-graphyne nanoribbon heterostructure. *European Physical Journal B*, 94:52, 2021.

[25] Duan, J., Wang, X., Lai, X., Li, G., Watanabe, K., Taniguchi, T., Zebarjadi, M. and Andrei, E. Y. High thermoelectric power factor in graphene/hBN devices. *PNAS*, 113(50):14272, 2016.

[26] Qin, D., Ge, X. –J., Ding, G. –Q., Gao, G. –Y. and Lu, J. –T. Strain-induced thermoelectric performance enhancement of monolayer $ZrSe_2$. *RSC Advances,* 7:47243, 2017.

[27] Hasdeo, E. W., Krisna, L. P. A., Hanna, M. Y., Gunara, B. E., Hung, N. T. and Nugraha, A. R. T. Optimal band gap for improved thermoelectric performance of two-dimensional Dirac materials. *Journal of Applied Physics,* 126:035109, 2019.

[28] Dean, C. R., Young, A. F., Meric, I., Lee, C., Wang, L., Sorgenfrei, S., Watanabe, K., Taniguchi, T., Kim, P., Shepard, K. L. and Hone, J. Boron nitride substrates for high-quality graphene electronics. *Nature Nanotechnology,* **5**:722, 2010.

[29] Xia, Y., Park, J., Zhou, F. and Ozolins, V. High thermoelectric power factor in intermetallic CoSi arising from energy filtering of electrons by phonon scattering. *Physical Review Applied*, **11**:024017, 2019.

[30] Blochl, P. E. Projector augmented-wave method. *Physical Review B*, 50:17953, 1994.

[31] Giannozzi, P., Baroni, S., Bonini, N., Calandra, M., Car, R., Cavazzoni, C., Ceresoli, D., Chiarotti, G. L., Cococcioni, M., Dabo, I., Corso, A. D., de Gironcoli, S., Fabris, S., Fratesi, G., Gebauer, R., Gerstmann, U., Gougoussis, C., Kokalj, A., Lazzeri, M., Martin-Samos, L., Marzari, N., Mauri, F., Mazzarello, R., Paolini, S., Pasquarello, A., Paulatto, L., Sbraccia, C., Scandolo, S., Sclauzero, G., Seitsonen, A. P., Smogunov, A., Umari, P., and Wentzcovitch, R. M. QUANTUM ESPRESSO: a modular and open-source software project for quantum simulations of materials. *Journal of Physics: Condensed Matter*, 21(39):395502, 2009.

[32] Perdew, J. P., Burke, K. and Ernzerhof, M. Generalized gradient approximation made simple. *Physical Review Letter*, 77:3865, 1996.

[33] Grimme, S. Semiempirical GGA-type density functional constructed with a long-range dispersion correction. *Journal of Computational Chemistry*, 27(15):1787–1799, 2006.

[34] Madsen, G. K. H. and Singh, D. J. BoltzTrap. A code for calculating band-structure dependent quantities. *Computer Physics Communication*, 175:67, 2006.

[35] Baral, D., Fu, Z., Zadorozhnyi, A. S., Dulal, R., Wang, A., Shrestha, N., Erugu, U., Tang, J., Dahnovsky, Y., Tian, J. and Chien, T. Small energy gap

revealed in CrBr3 by scanning tunnelling spectroscopy. *Physical Chemistry Chemical Physics*, 23:3225, 2021.

[36] Bahk, J.-H. and Shakouri, A. Enhancing the thermoelectric figure of merit through the reduction of bipolar thermal conductivity with heterostructure barriers. *Applied Physics Letter*, 105:052106, 2014.

[37] Karamitaheri, H., Pourfath, M., Faez, R. and Kosina, H. Geometrical effects on the thermoelectric properties of ballistic graphene antidot lattices. *Journal of Applied Physics,* 110:054506, 2011.

[38] Cutler, M. and Mott, N. F. Observation of Anderson Localization in an Electron Gas. *Physical Review*, 181:1336, 1968.

[39] Rosi, F. D. Thermoelectricity and thermoelectric power generation. *Solid-State Electronics*, 11:833, 1968.

[40] Suh, J. et al. Simultaneous Enhancement of Electrical Conductivity and Thermopower of Bi_2Te_3 by Multifunctionality of Native Defects. *Advanced Materials*, 27:3681, 2015.

[41] Fauque´, B., Butch, N. P., Syers, P., Paglione, J., Wiedmann, S., Collaudin, A., Grena, B., Zeitler, U. and Behnia, K. Magnetothermoelectric Properties of Bi2Se3. *Physical Review B*, 87:035133, 2013.

[42] Thanou-Christodoulaki, E., Papastaikoudis, C. and Mair, G. Quantum oscillations of the Nernst effect in single crystals of gallium. *Journal of Physics F: Metal Physics*, 12:1421, 1982.

[43] Stern, E. A. Rigid-Band model of alloys. *Physical Review*, 157:3, 1967.